Supplemental Material for Super-resolution microscopy of cold atoms in an optical lattice

Mickey McDonald, Jonathan Trisnadi, Kai-Xuan Yao, and Cheng Chin
James Franck Institute, Enrico Fermi Institute, and Department of Physics, The University of Chicago, Chicago, IL 60637, USA

I. EXPERIMENT SETUP

A. Preparation of cold atoms in an optical lattice

The experiment begins by loading a magneto-optical trap for 1 s with $\sim 2 \times 10^7$ ^{133}Cs atoms and performing molasses cooling to $\sim$10 μK. After, we turn on a 3D optical lattice (trap frequency $\approx$30 kHz) to perform degenerate Raman sideband cooling down to $<$1 μK, after which we are left with $\approx 2 \times 10^6$ atoms polarized in the $|F = 3, m_F = 3\rangle$ state with 90% occupancy in the motional ground state in the lattice direction (as determined by time-of-flight thermometry). After cooling, two axes of the 3D trapping lattice are adiabatically ramped off in 1 ms and the remaining trapping 1D lattice (spacing = $\lambda_{\text{trap}}/2$) is ramped to a chosen power which determines the single-site harmonic oscillator width. At this point the sample is ready for the super-resolution experiment.

B. Optical setup

To take full advantage of the nonlinear optical response described by Eq. (1), it is critical that the OP lattice has clean zero-intensity nodes. Due to small losses accumulated in the optical path (e.g. from windows, beamsplitters, etc.), the retro-reflecting beam diameter is made to be 84% the incident beam diameter so that incident and retro intensities can be closely matched. Additional fine tuning of the retro intensity is provided by adjusting its transmission through a polarizing beam splitter using a quarter waveplate QWP2 (Fig. S1). The retro intensity is optimized by maximizing the signal-to-noise of $\tilde{n}$ at $I/I_{\text{sat}} \gtrsim 1$.

Precise alignment of the OP and trapping lattices is necessary to minimize blurring due to angled moiré fringes. We do so by outputting both beams from the same optical fiber, and precisely aligning their retro-reflections via fiber back-coupling to within $\pm$ 20 μrad of optimal. This procedure is performed within a few hours before experiments are run to correct for mirror drift.

C. Dynamics

For the dynamics experiment described in Fig. 3, the 1D trapping lattice is translated by jumping the laser frequency by 56 MHz in $\sim$3 μs using an acousto-optic modulator (AOM). This corresponds to a positional shift of 79 nm of the lattice sites given a separation of 0.50 m between the atom cloud and the retro mirrors. After a variable hold time τ, the atomic density is sampled with the OP pulse as described above. The data presented in Fig. 3(b) are smoothed using a local low-order regression with a window of $\lambda_{\text{trap}}/20$ at each hold time τ. Note that while the entire imaging sequence spans 10 μs, the relevant signal is accumulated only during the 1.4 μs OP pulse, which allows for studies of fast $<$ 10 μs dynamics as described in the main text.

D. Moiré magnification

When imaging moiré patterns, the experimental procedure is identical to the generic super-resolution experiment, except that the retro mirror displacement is not varied. Post-processing to obtain $\mathcal{F}$ is identical, except no binning is used. The size of the camera pixels in the imaging plane is determined by dropping the cloud and comparing its acceleration to gravity. The moiré magnification M in Fig. 4(e) is obtained by dividing the real space distance between stripe centers (as fitted by Gaussians) by the lattice spacing $\lambda_{\text{trap}}/2$. Moiré-magnified dynamics are realized by performing the same lattice phase jump as described in Fig. 3.

E. Post-processing

Post-processing consists of binning each image (typically using 10-pixel wide squares). Bins with small atom number below a threshold have low signal-to-noise ratio and are therefore not analyzed. Due to a frequency difference between OP and trapping lattices, this 10-pixel binning contributes a small (few nm) blur in the signal. The size of 10 pixels is chosen to balance between good signal-to-noise and blurring. We obtain images of atoms with the OP lattice and a reference image with all atoms pumped to $|F = 4\rangle$ in order to determine the excitation fraction $\mathcal{F}$ for each bin.

F. Calibration of piezo displacement

Calibration of the piezo displacement Δx must be accurate to within nanometers in order to prevent systematic distortion of the signal. Here Δx is primarily

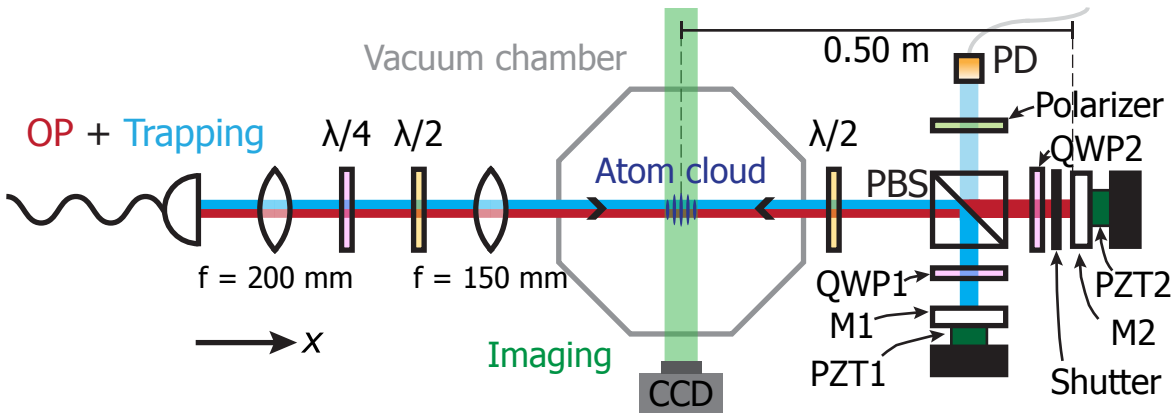

FIG. S1: **Optical setup for super-resolution experiment.** The 1D OP and 1D trapping lattices emerge from the same fiber to ensure good relative alignment. A polarizing beam-splitter (PBS) is used to separate the two beams, which are linearly polarized in orthogonal directions. The photodiode PD is used to calibrate the relative positions of the two retro-reflecting mirrors, which are both 0.50 m away from the atom cloud.

determined by the relative positions of the two retro-reflecting mirrors of the OP and trapping lattices, which are measured interferometrically every shot. To perform this measurement, we turn on the trapping lattice and make use of leakage light from the polarizing beam splitter shown in Fig. 1(b). The two arms of the polarizing beam splitter re-combine and interfere on a photodiode. A second piezo, attached to the trapping lattice mirror, is scanned over a few lattice spacings, and the phase (in nm) of the resulting sinusoidal signal on the photodiode is measured.

Additionally, a correction term to Δx is applied in order to account for position drift in the trapping lattice nodes due to frequency drift of the laser. The trapping lattice originates from a Ti:sapphire laser that is stable to ≈50 MHz/hour. The nodes of the lattice will shift by $(\Delta f_{\mathrm{tr}}/f_{\mathrm{tr}})L$ where Δf_{tr} is the change in frequency, $f_{\mathrm{tr}} = 351$ THz is the frequency of the trapping light, and L is the distance between the atom cloud and the retro-reflecting mirror. For our setup, $L = 0.50$ m so that the trapping nodes will shift at a rate of 1.4 nm/MHz. We calibrate the frequency drift of the trapping laser every shot by observing its peak position on a Fabry-Perot cavity relative to a stable reference laser to within 1 MHz.

G. Atom number drift

Since our signal is the excitation fraction, slow drift in total atom number is calibrated using a running reference image that is based on saturated atom images that are taken using a high-power OP beam without spatial structure (i.e. no lattice). These calibration shots are taken either every shot or every four shots, depending on the type of experiment we perform. The calibration shots are binned, and the reference image is calculated by applying a Savitsky-Golay filter to each bin using calibration shots nearby in time.

II. OPTICAL PUMPING UNDER SPATIALLY DEPENDENT DRIVE FIELD

Here we derive Eq. 1 in the main text, stating that the excitation fraction under a spatially dependent drive field is given by a convolution. The derivation is given assuming a pure initial state for the atom. Generalization to mixed states is straight forward.

The atom has spatial and electronic degrees of freedom. Therefore, a state can be written as

$$|\psi\rangle = \sum_{i,j} \psi_{i,j} |i\rangle_x \otimes |j\rangle_e, \tag{S1}$$

where $|i\rangle_x$ and $|j\rangle_e$ form a basis in the spatial and electronic subspace, respectively, and $\psi_{i,j}$ are the probability amplitudes.

A density matrix $\hat{\rho}$ can be written similarly:

$$\begin{aligned}\hat{\rho} &= \sum_{i_1,i_2,j_1,j_2} \rho_{i_1,i_2,j_1,j_2} |i_1\rangle_x\langle i_2|_x \otimes |j_1\rangle_e\langle j_2|_e \\ &= \sum_{\alpha,\beta} \rho_{\alpha,\beta} \hat{\alpha}_x \otimes \hat{\beta}_e.\end{aligned} \tag{S2}$$

Here each $\hat{\alpha}_x = |i_1\rangle_x\langle i_2|_x$ for some i_1, i_2, and notates a basis for the density matrix in the spatial subspace. Similarly $\hat{\beta}_e$ denotes a basis in the electronic subspace.

Optical pumping is described by a linear first order differential equation for the density matrix $\hat{\rho}$, in the form

$$i\partial_t\hat{\rho} = \mathcal{L}\hat{\rho}, \tag{S3}$$

where $\mathcal{L}$ is a linear operator on $\hat{\rho}$. This linear equation can be solved by matrix exponentiation:

$$\rho(t) = e^{-i\mathcal{L}t}\hat{\rho}(0) = U(t)\hat{\rho}(0), \tag{S4}$$

where the evolution operator $U(t) = e^{-i\mathcal{L}t}$ is the matrix exponentiation of $\mathcal{L}$.

Given the basis of $\hat{\rho}$, we can expand the linear operator U:

$$\begin{aligned} U &= \sum_{\alpha_1,\alpha_2,\beta_1,\beta_2} A_{\alpha_1,\alpha_2,\beta_1,\beta_2}(\hat{\alpha}_{1,x}\hat{\alpha}_{2,x}) \otimes (\hat{\beta}_{1,e}\hat{\beta}_{2,e}) \\ &= \sum_{u,v} A_{u,v}\hat{u}_x \otimes \hat{v}_e. \end{aligned} \tag{S5}$$

Here $\hat{u}_x$ and $\hat{v}_e$ again denote basis in the spatial and electronic subspace.

The excitation fraction is the probability of the atom to be found in a 'pumped' state $|p\rangle$ in the electronic subspace, and is given by

$$\mathcal{F} = \mathrm{Tr}(\hat{P}\hat{\rho}), \tag{S6}$$

where $\hat{P} = |p\rangle\langle p|$ is the projection operator onto $|p\rangle$. Therefore the excitation fraction after evolution U from a initial pure state $\hat{\rho}_0 = \hat{\rho}_{x,0} \otimes \hat{\rho}_{e,0}$ is

$$\begin{aligned} \mathcal{F} &= \mathrm{Tr}(\hat{P}U\hat{\rho}_0) \\ &= \mathrm{Tr}(\sum_{u,v} A_{u,v}\hat{u}_x\hat{\rho}_{x,0} \otimes \hat{P}\hat{v}_e\rho_{e,0}) \\ &= \sum_{u,v} A_{u,v}\mathrm{Tr}(\hat{u}_x\hat{\rho}_{x,0})\mathrm{Tr}(\hat{P}\hat{v}_e\rho_{e,0}) \\ &= \mathrm{Tr}\left(\left[\sum_{u,v} A_{u,v}\mathrm{Tr}(\hat{P}\hat{v}_e\rho_{e,0})\hat{u}_x\right]\rho_{x,0}\right) \\ &= \mathrm{Tr}\left(f\rho_{x,0}\right), \end{aligned} \tag{S7}$$

where we denote $f = \sum_{u,v} A_{u,v}\mathrm{Tr}(\hat{P}\hat{v}_e\rho_{e,0})\hat{u}_x$. This f is in fact the excitation fraction of atoms in a uniform drive field, as in that case spatial degree of freedom is decoupled and $\mathcal{F} = \mathrm{Tr}\left(f\rho_{x,0}\right) = f$. Noting that the action of f on $\rho_{x,0}$ is direct multiplication, we have

$$\mathcal{F}(\Delta x) = \int n(x)f(\Delta x - x)dx, \tag{S8}$$

where $n(x)$ is the diagonal of $\rho_{x,0}$ and is the initial spatial distribution, and $f(\Delta x - x)$ is the local excitation fraction due to an optical pumping lattice displaced by Δx. As the remaining fraction $g \equiv 1 - f$ and $\int n(x)dx = 1$, we derive Eq. 1 in the main text.

$$\begin{aligned} 1 - \mathcal{F}(\Delta x) &= 1 - \int n(x)\left[1 - g(\Delta x - x)\right]dx \\ &= \int n(x)g(\Delta x - x)dx. \end{aligned} \tag{S9}$$

III. THREE-STATE OPTICAL PUMPING MODEL

Here we derive Eqs. 2 and 3 in the main text through quantitatively describing the optical pumping process.

We consider the states $F = 3, 4, 4'$. Spontaneous emission of $F' = 4$ state does not always result in state $F = 4$, but also state $F = 3$. The branching ratio for the desired decay into $F = 4$ is $\beta = 7/12$. In addition, we always operate in the regime where the pulse duration is much longer than the natural lifetime $1/\Gamma$ of the $F' = 4$ state, such that Rabi oscillations can be neglected. Therefore we employ a three state rate equation model:

$$\begin{aligned} \dot{p_{4'}} &= -\frac{s\Gamma}{2}(p_{4'} - p_3) - \Gamma p_{4'} \\ \dot{p_3} &= -\frac{s\Gamma}{2}(p_3 - p_{4'}) + (1-\beta)\Gamma p_{4'} \\ \dot{p_4} &= \beta\Gamma p_{4'} \\ f &= p_4, \end{aligned} \tag{S10}$$

where p denote occupation probabilities for different internal states, the excitation fraction f is equal to the probability p_4 of the atom to be in $F = 4$ state, and $s = 2\Omega^2/\Gamma^2 = I/I_{\mathrm{sat}}$ is the laser intensity I in units of saturation intensity I_{sat}. We determine I_{sat} experimentally by fitting the scattering rate measured at different laser intensities.

Such a first order linear differential equation can be easily solved by matrix diagonalization. The solution of f at pulse time t and intensity s corresponding to drive field Ω is found to be:

$$\begin{aligned} f &= 1 - \frac{\gamma_+}{\gamma_+ - \gamma_-}e^{-\gamma_- t} - \frac{\gamma_-}{\gamma_- - \gamma_+}e^{-\gamma_+ t} \\ \gamma_\pm &= \frac{\Gamma}{2}(s+1)\left(1 \pm \sqrt{1 - 2s\beta/(s+1)^2}\right). \end{aligned} \tag{S11}$$

The optical pumping lattice formed by retro-reflecting a beam with intensity I gives rise to a drive field described by:

$$\Omega(x) = \sqrt{2s_0\Gamma^2}\sin(2\pi x/\lambda_{\mathrm{op}}), \tag{S12}$$

where $s_0 = I/I_{\mathrm{sat}}$ and $\lambda_{\mathrm{op}} = 852.335$ nm is the wavelength of the optical pumping light. In the limit of long pulse time $t \gg 1/\Gamma$ where we operate, we can consider only the case with $s \ll 1$, as elsewhere $f \approx 1$. In this case,

$$f = 1 - e^{-\frac{\beta\Gamma}{2}\frac{s}{s+1}t}, \tag{S13}$$

where $s = 2\Omega^2/\Gamma^2 = 4s_0\sin^2(2\pi x/\lambda_{\rm op})$. Therefore

$$g = e^{-\frac{\beta\Gamma}{2}\frac{s}{s+1}t}. \tag{S14}$$

The full width at half maximum w of $g(x)$ is given by equation $g(w/2) = g(0)/2$. In the regime of super-resolution where $w \ll \lambda_{\rm op}$, the solution is

$$w = \frac{\lambda_{\rm op}}{2\pi}\sqrt{\frac{2\ln 2}{s_0 t\beta\Gamma}}. \tag{S15}$$

This describes the predicted resolving power and its scaling with pumping power and pulse time in the strong pulse, long time limit.

The theoretical resolution shown in Fig. 2(c) in the main text is obtained differently, without making analytical approximations. Instead, the shown prediction is the FWHM of a numerically fitted Gaussian to the shape $f(x)$, the same way FWHM is extracted from experimental data.

IV. NUMERICAL SIMULATION OF MOTIONAL DYNAMICS

Dynamics of a single particle in a sinusoidal optical lattice is given by the Schroedinger equation:

$$i\hbar\partial_t\psi = -\frac{\hbar^2}{2m}\partial_x^2\psi - V_0\cos(4\pi x/\lambda)\psi. \tag{S16}$$

Given an initial condition ψ_0, this equation can be numerically solved by Fourier transform followed by matrix exponentiation, or projecting onto the basis of Mathieu functions, which are eigenstates of the Hamiltonian. We simulated the dynamics in a lattice with trap frequency 22.2 kHz, of an initial state that is the ground band Wannier function localized in one lattice site which is then shifted by 79 nm. The trap frequency was chosen to match the 21.64 kHz oscillation frequency extracted from a damped cosine fit to the red points in Fig. 2b. The resulting $|\psi(\tau)|^2$ is plotted against τ in the left part of Fig. S2. Comparing with measured data in Fig. 3(b), shown in the right part, simulation results reflect various features observed experimentally, including the non-sinusoidal motion of the peak, and the distortion of the wavefunction at later times. The simulation showed negligible tunneling to adjacent sites at 160 μs. Inhomogeneity of the traps along imaging direction is not included in simulation, and its contribution to damping of the observed dynamics cannot be reflected by the simulation.

V. IMAGING RESOLUTION

This section will describe several systematic sources of broadening in the super-resolution signal.

A. Probe width

The finite width of the super-resolution probe is determined by experimental parameters as described in the previous sections. The numerically predicted lineshape for a 1.4 μs pulse can be fitted with a Gaussian and plotted against I/Isat as shown in Fig. 2(c). For sufficiently high OP intensity, the width becomes smaller than that of the atomic density distribution.

B. Width of simple harmonic oscillator (SHO) thermal state

The absolute ground state of a simple harmonic oscillator (SHO) has a probability distribution with 1σ width given by $\sigma_0 = \sqrt{\hbar/2m\omega}$ where m is the mass of caesium and ω is the trap frequency. Since the atoms in our sample are not all in the ground state, but rather are in a thermal ensemble comprising of the ground state and excited states, the actual width will be broadened. This can be taken into account by computing the thermal state probability density distribution $P(x)$ via a Boltzmann-weighted sum of the SHO eigenstates. With distance in units of the harmonic oscillator length $\sqrt{\hbar/m\omega}$, the probability distribution of an atom in a thermal ensemble at temperature T can be written as:

$$P(x) = \frac{1}{Z}\sum_{n=0}^{\infty}\exp^{-E_n/k_BT}\left(\frac{1}{2^n n!}\pi^{-1/2}e^{-x^2}H_n(x)^2\right), \tag{S17}$$

where $Z = \left[2\sinh\left(\frac{hf}{2k_BT}\right)\right]^{-1}$ is the partition function, $E_n = \left(n+\frac{1}{2}\right)hf$ are the SHO energy eigenvalues, k_B is Boltzmanns constant, and $H_n(x)$ are the Hermite polynomials. Computing the sum shows that the distribution is Gaussian:

$$P(x) \propto \exp\left[-\left(1 - \frac{2e^{-hf/k_BT}}{1+e^{-hf/k_BT}}\right)x^2\right]. \tag{S18}$$

The 1σ width of the probability of an atom in a thermal ensemble with temperature T is given by:

$$\sigma(T) = \sigma_0\sqrt{\coth\left(\frac{hf}{2k_BT}\right)}. \tag{S19}$$

Using results from a time-of-flight temperature measurement, we compute the predicted ground and thermal state widths to be 40(2) and 45(2) nm, respectively (see Fig. 2(c)).

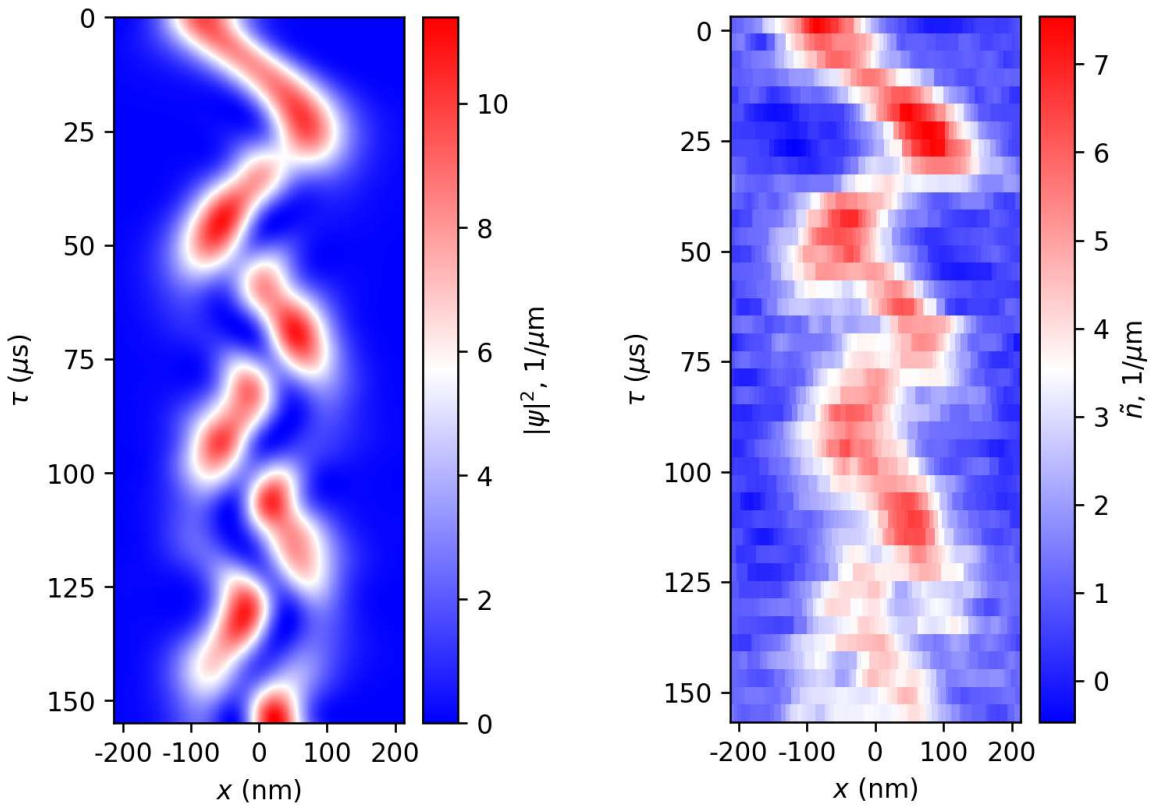

FIG. S2: Dynamics of an atom in a lattice site. Left: numerical simulation. Right: experimental data from Fig. 3(b).

C. Other systematic sources of blurring

a. Misalignment between OP and trapping lattices. Our absorption imaging scheme involves column integration of a 3-dimensional atom cloud onto the CCD plane. Suppose the two lattices are misaligned by an angle α, and the moiré pattern rotates by an angle $M\alpha$. Then, due to the different periodicities of the two lattices, the phase evolution across the cloud in the imaging direction z is given by

$$\phi(z) = \frac{\sin M\alpha}{M} z. \tag{S20}$$

Due to column integration, this effectively blurs the observed excitation fraction by a width

$$\sigma_\phi = \frac{\sin M\alpha}{M} \sigma_{\mathrm{at}}, \tag{S21}$$

where σ_{at} is the width of the atom cloud.

b. Binning. Since the trapping and OP lattices have a frequency difference δ, there is a linear phase gradient as shown in Fig. 4(b). The relative phase between the two lattices can be expressed (in units of length) as $\Delta\phi = \frac{\Delta f}{f} x = x/M$, where x is the position along the lattice direction and M is the same magnification as in Eq. 4. Since we wish to resolve spatial features of the atomic density, it is important to choose a bin width that is much smaller than $M\sigma(T)$. For the data presented in Fig. 2 with $\delta = 10$ GHz, a 10-pixel wide bin (corresponding to 61 μm on the cloud) samples over $\Delta\phi = 1.7$ nm, which is negligible compared to atomic feature sizes.